STARK DECELERATION AND TRAPPING OF OH RADICALS

Sebastiaan Y.T. van de Meerakker, Nicolas Vanhaecke, and Gerard Meijer

*Fritz-Haber-Institut der Max-Planck-Gesellschaft, 14195 Berlin, Germany;
email: basvdm@fhi-berlin.mpg.de, vanhaeck@fhi-berlin.mpg.de,
meijer@fhi-berlin.mpg.de*

Key Words cold molecules

■ **Abstract** The motion of polar molecules can be controlled by time-varying inhomogeneous electric fields. In a Stark decelerator, this is exploited to accelerate, transport, or decelerate a fraction of a molecular beam. When combined with a trap, the decelerator provides a means to store the molecules for times up to seconds. Here, we review our efforts to produce cold molecules via this technique. In particular, we present a new generation Stark decelerator and electrostatic trap that selects a significant part of a molecular beam pulse that can be loaded into the trap. Deceleration and trapping experiments using a beam of OH radicals are discussed.

1. INTRODUCTION

Getting better control over both the internal and external degrees of freedom of gas-phase molecules has been an important theme in molecular physics during the past decades. Molecular beams, both continuous and pulsed, are used throughout to produce large densities of molecules in selected quantum states (1). In these beams, the longitudinal temperature of the molecules is typically 1 K. State selection of a beam of (polar) molecules, and control over the orientation of the molecules in space, can be achieved by actively manipulating the transverse motion of the molecules using electrostatic or magnetic multipole fields, as well as with the help of laser radiation (1, 2, 3). Sophisticated and powerful detection schemes have been developed to experimentally study (half-) collisions (4, 5) and reactions (6, 7) of the thus prepared molecules in the required detail. Molecular beams have therefore been indispensable in a number of research areas, such as molecular (reactive) scattering studies, high-resolution spectroscopy, and surface science, as well as, for instance, the production and investigation of transient species. Until recently, it was difficult to obtain full control over the longitudinal motion of molecules in a molecular beam. The mean velocity of the beam can be varied by adjusting the temperature of the source or by using different seed gases, allowing the production

of beams in the 250–3000 m s^{-1} range. However, more precise control over the longitudinal motion, i.e., the ability to vary the velocity (distribution) of the beam to any desired (low) value, was not possible until the development of the so-called Stark deceleration technique. The Stark decelerator for neutral polar molecules is the equivalent of a linear accelerator (LINAC) for charged particles. In a Stark decelerator, the quantum state specific force that a polar molecule experiences in an electric field is exploited. This force is rather weak, typically some eight to ten orders of magnitude weaker than the force that the corresponding molecular ion would experience in the same electric field. This force nevertheless suffices to achieve complete control over the motion of polar molecules, using techniques akin to those used for the control of charged particles. This has been explicitly demonstrated by the construction of two types of linear accelerators (8, 9), a buncher (10), two types of traps (11, 12), and a storage ring (13) for neutral polar molecules.

With the Stark decelerator, a part of a molecular beam can be selected and transferred to any arbitrary velocity, producing bunches of state-selected molecules with a computer-controlled velocity and with longitudinal temperatures as low as a few mK (14, 15). When the Stark decelerator is combined with an electrostatic trap, bunches of state-selected polar molecules can be brought to a standstill and stored in the trap for times up to seconds. These experiments are of particular interest to the field of cold molecules, as the Stark deceleration technique is one of the few techniques that offers the possibility of confining ground-state molecules in a trap. Recently, extensive overviews of cold molecule production techniques have appeared (15, 16). Therefore, we confine this review to an overview of the experiments that have been conducted by us and other groups using Stark decelerators. In the second part of this review we discuss a Stark decelerator and an electrostatic trap that allow the deceleration and electrostatic trapping of a large fraction of a molecular beam. The operation of the decelerator and trap is demonstrated using a beam of OH radicals.

Interest in the field of cold molecules is triggered by various potential applications and by the promise of the occurrence of interesting new physics (and chemistry!) at the low temperatures and high densities that can ultimately be achieved. In the following, we give a brief summary of a selection of proposed experiments.

The resolution in a spectroscopic experiment can greatly benefit from the increased interaction time that decelerated molecular beams and/or trapped molecules offer. Cooling and confinement of molecules in the mK range improve the attainable resolution by orders of magnitude compared to the resolution that is obtainable for thermal molecules. This is generally important to study the molecules in the most detail, and it is essential for the great promise that the use of cold molecules holds in metrology, i.e., in experiments aimed at testing fundamental symmetries. For instance, it is expected that the most sensitive measurement of a possible electric dipole moment (EDM) of the electron can be performed on a polar molecule because of the large enhancement of electric fields inside the molecule. The existence of an EDM would have profound consequences for our

understanding of the evolution of the universe, and would test the standard model
(17). The molecules YbF and PbO are of particular interest for this (18, 19). The
improved resolution can also be used to study the difference in the energy levels between two enantiomers of a chiral molecule that could be a manifestation
of the weak interaction in molecules (20, 21). Such an energy difference could
explain the imbalance between D- and L-amino acids in biochemical systems.
Precise measurements of ro-vibrational transitions in molecules that have a strong
dependence on the proton-electron mass ratio (m_p/m_e) could be used to measure
a possible time dependence of fundamental constants, which would be a consequence of the expansion of the universe (22). Apart from the obvious benefits
in high-resolution spectroscopy, the long interaction times allow the direct measurement of the lifetime of an electronically or vibrationally excited state. With
conventional molecular beam techniques, the determination of these lifetimes is
limited to a few milliseconds. By measuring the temporal decay of the population
of vibrationally excited OH radicals in an electrostatic trap, we recently obtained
an accurate value for the Einstein *A*-coefficient of the fundamental 1–0 band of
OH (23). This measurement benchmarks the infrared radiative properties in the
Meinel system of OH that is of particular atmospheric and astrophysical importance
(24–27).

When particles are brought to (ultra-)low temperatures, the de Broglie wavelength associated with the wave character of the particles can become comparable
to, or even larger than, the inter-particle separation. In this exotic regime, interesting phenomena can be expected that are governed by quantum physics and that
are foreign to processes that take place at higher temperatures. In this respect, the
ability to cool and slow atoms with light for subsequent trapping (28–30) has led
to exciting and sometimes unforeseen results, and the payoffs include atom interferometry, precision spectroscopy, Bose-Einstein condensation, and the formation
of atom lasers (31, 32). Laser cooling and the techniques to further cool the atoms
have therefore revolutionized atomic physics over the last two decades. Methods
to cool and trap molecules have the potential to do the same for molecular physics.
Using molecules would add extra dimensions to these experiments as they can be
prepared in a wide variety of selected rotational and vibrational quantum states and
as they can be spatially oriented. Arguably one of the most interesting properties
of molecules that are foreign to atoms is that a molecule can possess a permanent
EDM. Ultra-cold polar molecules are therefore currently at the center of theoretical
and experimental interest. The anisotropic long-range dipole-dipole interaction in
a molecular Bose-Einstein Condensate (BEC) is predicted to give the molecular
condensate new and intriguing properties. If the dipoles are oriented head-to-tail,
the dipole-dipole interaction is attractive, whereas this interaction is repulsive for
oriented dipoles in lateral geometry. In a polarized bosonic gas, the stability of
the BEC therefore depends on the geometry of the trap (33). By changing the
geometry of the trap, one has the possibility of tuning the interactions in the gas,
offering new possibilities to engineer macroscopic quantum states (34). Furthermore, the use of trapped dipolar molecules in an optical lattice has been proposed

to study exotic quantum phase transitions (35), as well as quantum computation (36).

The study of chemistry at ultra-low temperatures is another exciting avenue. Cooling molecules to (ultra-)low temperatures gives access to an exotic regime for chemical reactivity, governed by quantum tunneling and resonances (37, 38). Interesting effects are predicted to occur for collisions at low energies of collision. The elastic and inelastic cross sections show sharp resonances at these energies (39). Unusual resonant states can be formed when the colliding molecules begin to rotate, leaving them with insufficient translational energy to overcome their van der Waals attraction, effectively binding the molecules transiently together. The slow (or trapped) molecules produced by a Stark decelerator are particularly amenable to these kind of experiments. In a molecular (reactive) scattering experiment using crossed Stark-decelerated molecular beams of identical or different species, for instance, the scattering process can be studied as a function of the collision energy, probing the potential energy surface with unprecedented detail. These new kinds of experiments are complementary to conventional spectroscopy of collision complexes and to molecular beam scattering experiments at relatively high-collision energies.

2. STARK DECELERATION OF A MOLECULAR BEAM

Analogous to the transverse focusing of a molecular beam using transversally inhomogeneous electric fields, the longitudinal velocity of a beam of polar molecules can be changed using longitudinally inhomogeneous electric fields. The longitudinal velocity of a molecular beam is typically too large, however, to enable a significant change of the velocity in experimentally attainable electric fields. In addition, as the molecule leaves the region of high field, the velocity change is canceled. If, however, time-varying inhomogeneous electric fields are used, this situation can be avoided. When the electric field is reduced before the molecule has left the region of high electric field, the velocity of the molecule will not return to its original value and can therefore be permanently changed. When this process is repeated using multiple electric field stages, the longitudinal velocity of the beam can be changed to any desired value. This idea was already considered in the late 1950s and 1960s (40–44). Although even large-scale efforts were undertaken, the deceleration or acceleration of polar molecules could not be demonstrated (45–47), mainly due to lack of flexibility of the constructed machines. In recent years, our group has successfully developed the Stark deceleration technique. For the first time, the deceleration of neutral polar molecules, using time-varying inhomogeneous electric fields, could be demonstrated (8). The development of fast semiconductor high-voltage switches allows the use of an array of high-voltage electrodes that are equally spaced, greatly improving the flexibility of the device. In addition, the advent of pulsed supersonic molecular beams provides a source of high densities of molecules distributed over only a small number of internal

quantum states and with a narrow velocity distribution that is ideal to be injected in the decelerator. By employing a properly chosen sequence of switch times, the final velocity of the beam can be selected. Pulsed molecular beams with a computer-controlled velocity and with a narrow velocity distribution can thus be produced. This will be of advantage for the use of decelerated molecular beams in any molecular beam experiment where the velocity, or velocity distribution, of the molecules is an important parameter.

2.1. Previous Work Using Stark Decelerators

The possibility of decelerating a beam of neutral polar molecules with an array of time-varying inhomogeneous electric fields was first demonstrated by Bethlem et al. in 1999 (8). In this work, a small part of a pulsed beam of CO molecules in their metastable $a\,^3\Pi$ state was slowed down from 225 m s^{-1} to 98 m s^{-1} using a 35 cm long Stark decelerator that consisted of 63 electric field stages. The similarity of the Stark decelerator for neutral molecules with a LINAC for charged particles, and in particular the demonstration that molecular motion through the Stark decelerator is also governed by the concept of phase stability, was demonstrated one year later, again using a beam of metastable CO molecules (48). This is important as it clearly demonstrates the potential of the Stark decelerator for transferring the high initial phase-space density of molecules in the appropriate quantum state that is present in a molecular beam to any desired laboratory velocity, without loss. The description of longitudinal phase stability has since then been refined including higher-order terms in the analysis (49, 50). It was shown that these higher-order terms can lead to additional phase-stable regions (49). A detailed analysis of the transverse stability, and of the coupling between the transverse and longitudinal motion has also been given (51). In some cases, this coupling can lead to unstable trajectories that significantly reduce the acceptance of the decelerator, whereas in other situations the acceptance is actually enhanced. The existence of the additional phase-stable regions, and the influence of the transverse motion on longitudinal phase stability, has experimentally been verified using a beam of OH radicals (49, 51).

In 2000, the same decelerator that was used in the CO experiments was used to decelerate ground-state ND$_3$ molecules to a standstill and to subsequently trap these molecules in a quadrupole electrostatic trap (11). A more detailed description of the Stark decelerator and the trap-loading process was published two years later (14). Meanwhile, an electrostatic storage ring that allows the confinement of a slow molecular packet in two dimensions was designed and constructed. In this prototype storage ring, packages of ammonia molecules, traveling with a velocity of about 100 m s^{-1}, could be observed up to six round trips (13). A buncher, an element that allows one to longitudinally focus a molecular beam (either spatially or in velocity space), was developed and used to spatially focus a decelerated beam of deuterated ammonia, as well as to create a molecular beam with a record-low longitudinal temperature of 250 μK (10). Recently, this buncher has been installed

between the Stark decelerator and the storage ring to enable the injection of colder packages in the ring; the number of observable round trips could be increased to more than 50 (52). A second Stark decelerator, which is identical to the initial design but with an increased number of 95 deceleration stages, was constructed to demonstrate the improved spectroscopic resolution that can be obtained when using Stark-decelerated molecular beams (53). After deceleration of a beam of ND_3 to approximately 50 m s^{-1}, the spectral width of individual hyperfine transitions, determined by transit-time broadening in the 6.5 cm long microwave interaction zone, could be reduced to approximately 1 kHz. The hyperfine structure on the inversion doubling transition in the $|J,K\rangle = |1,1\rangle$ state of $^{15}ND_3$ could be completely resolved and analyzed. This method has also been used to produce slow $^{15}ND_3$ molecules in the high-field seeking $|J,K\rangle = |1,1\rangle$ state that could subsequently be trapped in an AC electric field trap (12). This is the first trap of its kind for molecules in their absolute ground state. The strong dipole-dipole interaction between polar molecules is predicted to lead to high loss rates from the trap if the molecules are electrostatically trapped in a low-field seeking state (54), and the development of the AC trap is therefore expected to be essential for the demonstration of evaporative cooling. The manipulation of polar molecules using miniaturized electrode geometries and only modest voltages has been investigated as well. In a proof-of-principle experiment, a beam of ammonia molecules was retro-reflected from a planar array of 20 μm wide gold electrodes, spaced 20 μm apart, on a sapphire substrate (55). With a voltage difference of only 350 V between adjacent electrodes, the microstructure acts as a flat mirror for ND_3 molecules with a velocity as high as 30 m s^{-1}.

All molecular beam deceleration experiments described above have been performed with molecules in so-called low-field seeking states, i.e., molecules that experience an appreciable positive Stark shift in experimentally attainable electric fields. Although this covers a relatively large class of polar molecules, many interesting molecules, in particular large or massive polar molecules, exclusively exhibit high-field seeking states. In addition, the absolute ground state of any polar molecule is high-field seeking. Deceleration of molecules in a high-field seeking state in the Stark decelerator is in principle straightforward, but the molecules are attracted to the region where the fields are the highest. Therefore, high-field seeking molecules have the tendency to crash into the electrodes. An electrode geometry that produces a maximum of the electric field in three dimensions, required to solve this fundamental problem, is not possible (Earnshaw's theorem). A scheme that is well known from charged particle accelerator physics, where the same principle difficulty exists, can be used to advantage, however. By alternately focusing and defocusing molecules in each transverse direction, a net overall focusing of a beam of molecules in a high-field seeking state can be obtained. A prototype of an alternating gradient (AG) decelerator with only 12 electric field stages has been constructed to demonstrate focusing and deceleration of metastable CO molecules in a high-field seeking state (9) in 2002. A mechanically improved version of this decelerator has subsequently been used to decelerate a beam of YbF molecules

(56). As mentioned in Section 1, YbF is of particular interest because it offers one of the most sensitive ways to search for elementary particle physics beyond the standard model through a measurement of the EDM of the electron (18). By using a decelerated molecular beam, the precision with which this quantity can be measured can greatly be enhanced. When sufficient electric field stages are employed in these AG decelerators, in principle the molecules can be decelerated to rest. In combination with the AC electric trap discussed before (12), potentially any polar molecule, including biomolecules, can then be decelerated and trapped.

Since the introduction of the Stark decelerator in 1999, various research groups have followed this experimental approach with the aim of producing samples of cold molecules. Of these, the group of Jun Ye at JILA in Boulder, Colorado, has successfully implemented the method in recent years. Using a design that is identical to the original design of the decelerator, the possibility of manipulating the phase-space distribution of OH radicals in a Stark decelerator was demonstrated (57), and the deceleration of part of a beam of OH radicals from 385 m s^{-1} to 58 m s^{-1} was shown (58). The group of Tiemann and Lisdat in Hannover, Germany, are constructing a (long) Stark decelerator with the aim to decelerate a beam of SO_2 molecules to subsequently produce slow SO radicals via photodissociation (C. Lisdat, private communication). Another Stark decelerator is currently under construction in the group of Softley in Oxford. A long decelerator of the AG type with the aim to decelerate YbF molecules to rest has just been completed in the group of Hinds and Tarbutt at Imperial College in London.

Inspired by the manipulation of polar molecules in a Stark decelerator, studies on the manipulation of atoms and molecules in high Rydberg states with electric fields were recently performed. Compared to the polar molecules used in a Stark decelerator, atoms or molecules in a Rydberg state offer a much larger EDM. Hence, these particles can be efficiently manipulated using only modest electric field strengths in a single or a few electric field stages. These methods have been pioneered using H_2 molecules (60) and Ar atoms (61). Sophisticated schemes in which the electric field continuously follows the motion of the particles, and hence allows phase-stable deceleration, have been proposed as well (62). The disadvantages of these decelerators are that the atoms or molecules need to be prepared in the Rydberg states using sophisticated laser systems and that the lifetime of the Rydberg states severely limits the time available to bring the molecules to rest and to store them in a trap.

The interaction of polar molecules with an electric field has also been exploited in schemes to filter out the slow molecules from a thermal gas. Using a linear electrostatic quadrupole guide with a curved section, samples of slow H_2CO and ND_3 molecules, in a large number of quantum states, have been selected from the low-velocity tail of a Maxwellian distribution of a room-temperature effusive source (63), a successful reincarnation of the Zacharias fountain. (The work of J.R. Zacharias has never been published, but knowledge of the Zacharias fountain has been passed down in the oral tradition.) More recently, AC voltages have been

applied to the guide to (in principle) select ND_3 molecules in both low-field seeking and high-field seeking states (65).

An optical analog of the Stark decelerator has been proposed as well (66, 67). In this scheme, the interaction of polarizable molecules with a high-intensity pulsed optical lattice, produced by two counter-propagating laser beams, is utilized. By chirping one of the beams, the lattice velocity can be reduced from the mean velocity of a molecular beam to any desired final velocity. In a recent proof-of-principle experiment, a single-stage optical Stark decelerator has been used to reduce the velocity of a beam of benzene molecules from 320 m s^{-1} to 295 m s^{-1} (68).

2.2. Phase Stability in a Stark Decelerator

The operation principle of a Stark decelerator and a description of phase stability are given in detail in References 8, 14, and 48. The description is only briefly repeated here. The decelerator consists of an array of electric field stages centered a distance L apart, as schematically represented in Figure 1. Opposing electrodes
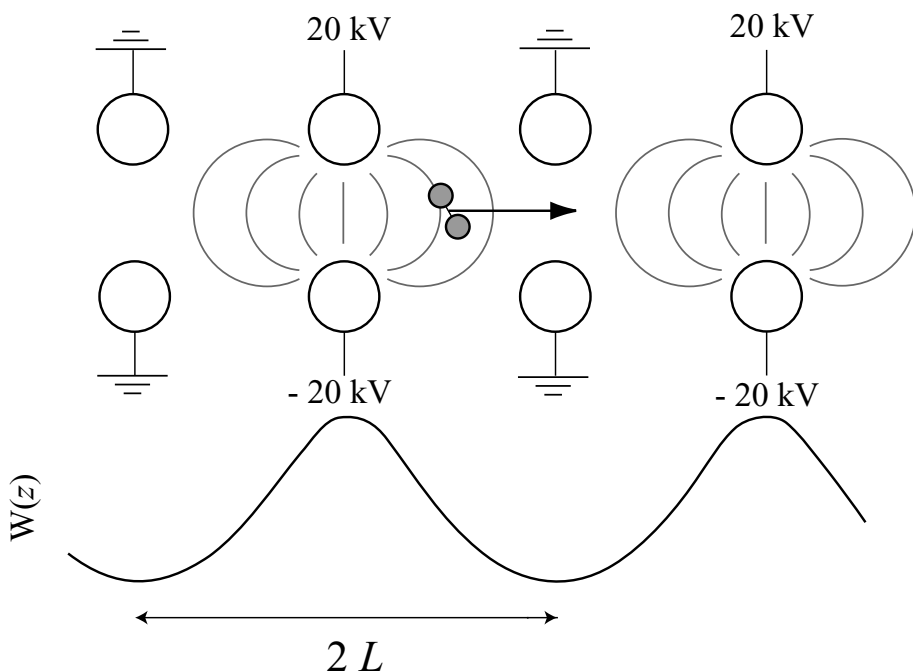
Figure 1   Scheme of the Stark decelerator, together with the Stark energy of a molecule as a function of position z along the molecular beam axis. Adjacent electric field stages are spaced a distance $L = 11$ mm apart. Each electric field stage consists of two parallel 6 mm diameter cylindrical rods with a center-to-center distance of 10 mm. A maximum voltage difference of 40 kV is applied to opposing rods in an electric field stage.

are connected to a switchable power supply with different polarity. All alternating electric field stages are electrically connected to each other. When the odd electrodes are switched to high voltage, the even electrodes are switched to ground and vice versa. At a given time t, the potential energy of a polar molecule as a function of its position z has periodicity $2L$. It is therefore convenient to describe the motion of a molecule in terms of its reduced position $z\pi/L$, which has periodicity 2π. The energy a molecule loses per stage depends on its position at the time the fields are switched. This position is indicated by the phase angle ϕ (8, 14, 48). We define the position $\phi = 0$ at the position in between two adjacent pairs of electrodes such that the electrodes at $\phi = \pi/2$ are grounded just after the fields are switched.

By definition, a molecule with velocity v_0 is called synchronous if its phase ϕ_0 on the potential is always the same at the time the fields are switched, i.e., ϕ_0 remains constant and the molecule will lose a constant amount of kinetic energy per stage. The synchronous molecule achieves this by traveling exactly a distance L in the time ΔT between two successive switch times. This means that the synchronous molecule is always in phase with the switching of the decelerator. A molecule that has a slightly different phase ϕ and/or velocity v than the synchronous molecule will experience an automatic correction toward the equilibrium values ϕ_0 and v_0. For instance, a molecule that has a phase slightly higher than ϕ_0 at a certain switch time will lose more kinetic energy than the synchronous molecule, and the molecule will slow down with respect to the synchronous molecule. Its phase will get smaller, until it lags behind, after which the process reverses. Molecules within a certain region in phase space, bounded by the so-called separatrix, will undergo stable phase-space oscillations around the synchronous molecule. This mechanism is called phase stability and ensures that a package of molecules is kept together in the Stark decelerator throughout the deceleration process.

To derive the longitudinal equation of motion of molecules through the Stark decelerator, we will consider molecules that move along the molecular beam axis of the decelerator. The Stark energy of a molecule $W(z\pi/L)$ is symmetric around the position of a pair of electrodes and can conveniently be written as a Fourier series:

$$W(z\pi/L) = \frac{a_0}{2} + \sum_{n=1}^{\infty} a_n \cos(n(z\pi/L + \pi/2)). \qquad 1.$$

By definition, the synchronous molecule travels a distance L in the time ΔT between two successive switch times. The change in kinetic energy per stage $\Delta K(\phi_0) = -\Delta W(\phi_0)$ for a synchronous molecule with phase ϕ_0 and velocity v_0 at a certain switch time is then given by the difference in potential energy at the positions $z\pi/L = \phi_0$ and $z\pi/L = \phi_0 + \pi$:

$$\Delta W(\phi_0) = W(\phi_0 + \pi) - W(\phi_0) = 2a_1 \sin\phi_0. \qquad 2.$$

In the Stark decelerator, one repeatedly switches between two static situations. This is represented by the variable ϕ that is only defined when the fields are switched and $z\pi/L$ whose origin jumps by π every time the fields are switched.

However, to derive the equation of motion, continuous variables are required. If the deceleration rate is small compared to the kinetic energy of the molecule, we can regard the lost kinetic energy of the synchronous molecule between two successive switch times as the result of a continuously acting average force $\bar{F} = -\Delta W/L$. This approximation is equivalent to assuming that the phase of the synchronous molecule ϕ_0 is not only constant (and defined) at a switch time, but is also constant for the time in between two successive switch times. In this picture, the repeated switching of the potential between two static situations after a time interval ΔT is replaced by a traveling potential well that moves with velocity $L/\Delta T$. An equation of motion can then be derived that describes the motion of molecules through the Stark decelerator.

Within these approximations, the average force $\bar{F}$ that acts on the synchronous molecule is simply

$$\bar{F}(\phi_0) = \frac{-\Delta W(\phi_0)}{L} = -\frac{2a_1}{L} \sin\phi_0 \qquad\qquad 3.$$

if we only take the leading terms up to $n = 2$ in Equation 1 into account. The average force acting on a nonsynchronous molecule with a phase $\phi = \phi_0 + \Delta\phi$, but with a velocity v_0, is given by $-\frac{2a_1}{L} \sin(\phi_0 + \Delta\phi)$, and the equation of motion with respect to the synchronous molecule is

$$\frac{mL}{\pi} \frac{\mathrm{d}^2 \Delta\phi}{\mathrm{d}t^2} + \frac{2a_1}{L}(\sin(\phi_0 + \Delta\phi) - \sin(\phi_0)) = 0, \qquad\qquad 4.$$

where m is the mass of the molecule.

In the phase-stability diagrams of Figure 2, lines of constant energy are shown that result from a numerical integration of Equation 4 for OH radicals in the $J = 3/2, M\Omega = -9/4$ state and for the decelerator used in the present experiments. The equilibrium phase angles $\phi_0 = 0°$ and $\phi_0 = 70°$ for the synchronous molecule are used. The solid lines indicate the trajectories in phase space that molecules
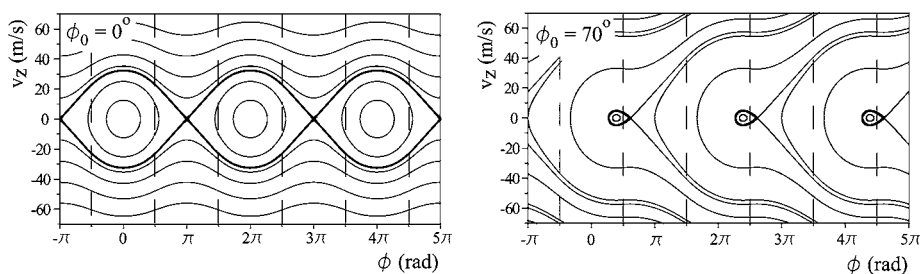
Figure 2 Phase stability diagram for OH ($J = 3/2$, $M\Omega = -9/4$) radicals when the decelerator is operated at a phase angle of $\phi_0 = 0°$ or $\phi_0 = 70°$. The positions of the electrodes of the decelerator are indicated by the dashed lines; a phase difference of 2π corresponds to a distance of 22 mm.

will follow. The positions of the electrodes of the decelerator are indicated by the vertical dashed lines. In the decelerator that is used here, a phase difference of 2π corresponds to a distance of 22 mm, a factor of 2 larger than the corresponding distance in Stark decelerators of earlier designs. Closed curves in the phase-space diagram correspond to bound orbits; molecules within the so-called bucket bound by the thick contour (called separatrix) will oscillate in phase space around the phase and velocity of the synchronous molecule. It is noted that operation of the decelerator at $\phi_0 = 0°$ corresponds to transporting (part of) the beam through the decelerator without deceleration, whereas acceleration and deceleration of the beam occurs for $-90° < \phi_0 < 0$ and $0 < \phi_0 < 90°$, respectively.

3. THE STARK DECELERATOR

In principle, the technique of Stark deceleration as described in Section 2.2 can be applied to any polar molecule that experiences a positive Stark shift in an applied electric field. In the first experiments, Stark decelerators were used that could only select and decelerate a relatively small fraction of a molecular beam. To exploit the possibilities that these slow molecular beams offer, the fraction of the pulsed molecular beam that is decelerated and/or trapped needs to come closer to unity, i.e., the six-dimensional phase-space acceptance of the various elements needs to be increased to better match the typical emittance of a molecular beam. In addition, for collision and reactive scattering experiments, the deceleration and trapping needs to be performed on those molecules that are chemically most relevant. We therefore set out to decelerate and trap a beam of ground-state OH ($X\,^2\Pi_{3/2}$, $J = 3/2$) radicals, using a new generation molecular beam deceleration and trapping machine, designed such that a large fraction of the molecular beam pulse can be captured.

The role of the omnipresent OH radical as intermediate in many chemical reactions, and in particular its major importance to astrophysical (69), atmospheric (24), and combustion (70) processes, has made this a benchmark molecule in collision and reactive scattering studies (71). The ability to decelerate and/or confine OH radicals in a trap offers the possibility of studying these processes with unprecedented detail. Triggered by this, the interaction between OH radicals at (ultra-)low temperatures and its implications for (ultra-)low-temperature chemistry is currently at the center of theoretical interest (72). Indeed, theoretical investigations predict fascinating processes will occur that are foreign to collisions at higher temperatures. In particular, in the presence of an electric field, the long-range dipole-dipole interaction between two OH radicals generates a shallow potential that supports bound states of the excited [OH]$_2$ dimer (73, 74). The existence of these so-called field-linked states depends very critically on the value of the field strength, offering the unique possibility of controlling the collision process by varying the electric field strength. As the OH radical possesses a relatively large magnetic dipole moment, it can in principle be magnetically trapped as well (75). This leaves the electric field

strength as a free parameter to control the collision process (57). The Stark deceleration and electrostatic trapping technique can also be used to confine fermionic OD radicals, in which case inelastic collisions between the trapped molecules that lead to trap loss are suppressed (76).

3.1. Experimental Setup

The experiments described here are performed in a molecular beam machine, schematically shown in Figure 3, that consists of three differentially pumped vacuum chambers. The source, deceleration, and detection chamber are pumped by a 1400 l s^{-1} (Pfeiffer Vacuum TMU 1600 M), 2 × 400 l s^{-1} (TMU 400 M), and a 400 l s^{-1} turbo molecular drag pump, respectively. The oil-free turbo pumps are equipped with magnetic bearings to make the vacuum system compatible with radical production methods that rely on the use of corrosive gases as a precursor. A pulsed beam of OH radicals is produced by photodissociation of HNO$_3$ molecules that are co-expanded with a rare gas through a room-temperature pulsed solenoid valve (General valve, series 9). The dissociation takes place at the tip of a quartz capillary that is mounted on top of the nozzle. In the experiments, either Kr or
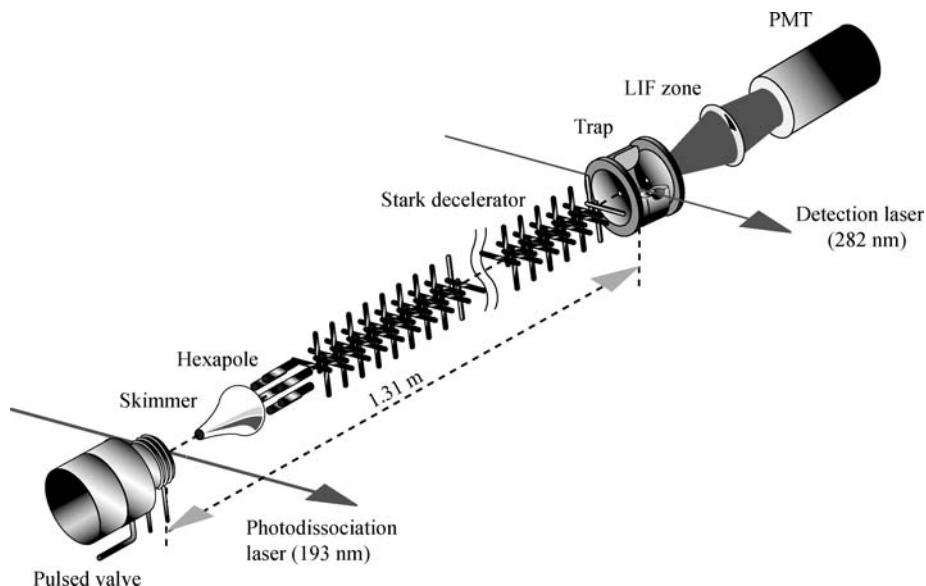
Figure 3   Scheme of the experimental setup. A pulsed beam of OH with a mean velocity of 450 m s^{-1} is produced via ArF-laser photodissociation of HNO$_3$ seeded in Kr. The molecular beam passes through a skimmer, hexapole, and Stark decelerator into the electrostatic quadrupole trap. State-selective laser-induced fluorescence detection is used to measure the density of the OH ($J = 3/2$) radicals at the center of the trap.

Xe is used as a seed gas, resulting in a mean velocity of the beam of around 450 m s^{-1} (Kr) or 360 m s^{-1} (Xe) with a velocity spread (FWHM) of about 15%. In the supersonic expansion, the beam is rotationally and vibrationally cooled, and after the expansion most of the OH radicals reside in the lowest rotational ($J = 3/2$) and vibrational level of the electronic ground state $X\,^2\Pi_{3/2}$. This level has a Λ-doublet splitting of 0.055 cm^{-1} and each Λ-doublet component is split into a $|M_J| = 1/2$ and a $|M_J| = 3/2$ component when applying an electric field. The $|M_J| = 3/2$ component offers a three times larger Stark shift than the $|M_J| = 1/2$ component. In the experiments described here, only the $M_J\Omega = -3/4$ and $M_J\Omega = -9/4$ components of the low-field seeking upper Λ-doublet component of f parity are of interest. The molecular beam passes through a 2.0 mm diameter skimmer placed 21 mm from the capillary and enters the second vacuum chamber. The experiment runs at a repetition rate of 10 Hz, and during operating conditions the pressure in the source and decelerator chambers is typically 2×10^{-5} and 4×10^{-7} torr, respectively.

In the decelerator chamber, the beam of OH radicals enters a 37 mm long hexapole 23.5 mm from the skimmer. The hexapole consists of six stainless steel rods with 3 mm diameter, placed equidistantly on the outside of a circle with a diameter of 6 mm. Alternating rods are electrically connected to each other. One set of rods is actively grounded, whereas the other set can be switched to high voltage, using a high-voltage power supply (Spellman SL150) in combination with a fast high-voltage switch (Behlke Elektronik HTS 151-03-GSM). When a high-voltage pulse is applied to the hexapole, the electric field inside the hexapole is zero on the molecular beam axis and increases quadratically with radial distance r from the beam axis (1, 77). Molecules in a low-field seeking state therefore experience a restoring force toward the molecular beam axis. For these states, a hexapole acts as a positive lens, and the divergence of the molecular beam can be reduced. The Stark effect of the $X^2\Pi_{3/2}$, $J = 3/2$, f state of OH is (nearly) linear, resulting in a (nearly) linear restoring force. For low electric fields close to the beam axis, however, the Stark effect is quadratic, causing aberrations of the hexapole lens (78). In the experiments reported here, the hexapole is used to optimize the (transversal) in-coupling of the beam of OH radicals into the Stark decelerator. The importance of this phase-space matching is explained in detail in Reference 14. The hexapole is switched on (off) when the beam enters (exits) the hexapole. The voltage on the hexapole is set to maximize the signal of the selected package of OH radicals that exits the decelerator. In most experiments, the hexapole is operated between 10 and 14 kV, resulting in approximately a factor 3 increase in signal intensity, relative to when the hexapole is not used.

To minimize the longitudinal spreading out of the beam, the Stark decelerator is placed only 16.8 mm from the exit of the hexapole, limiting the total distance from the nozzle orifice to the Stark decelerator to less than 10 cm. The Stark decelerator consists of an array of 108 equidistant electric field stages, with a center-to-center distance L of adjacent stages of 11 mm. Each stage consists of two parallel 6 mm diameter polished hardened-steel rods that are centered 10 mm

apart, symmetrically around the beam axis. All alternating stages are rotated by $90°$ with respect to each other, providing a 4×4 mm^2 spatial transverse acceptance area. The geometry of this decelerator is scaled up by a factor of 2 compared to earlier designs, increasing the spatial acceptance of the decelerator by a factor of 2^3. This up-scaling has been performed while keeping the electric fields in the decelerator the same. The electrodes of the decelerator are positioned relative to the molecular beam axis within a specified precision of 0.05 mm. The decelerator is operated using a voltage of ± 20 kV between opposing electrodes in a field stage, creating a maximum electric field strength near the electrodes of 115 kV cm^{-1}. A picture of the decelerator, with a close-up of the 4×4 mm^2 opening area between the electrodes, is shown in Figure 4.

The high-voltage pulses can be applied to the electrodes using fast high-voltage switches (Behlke Elektronik HTS 651-03-GSM) that have been specifically developed for the decelerator described here. The individual electrodes of alternating stages are electrically connected to a single high-voltage switch, requiring a total of four independent switches for the decelerator. During a single time sequence, the high voltage is delivered by a 300 nF capacitor bank, limiting the voltage drop during a burst to better than 3%. Depending on the experiment, the duration of a
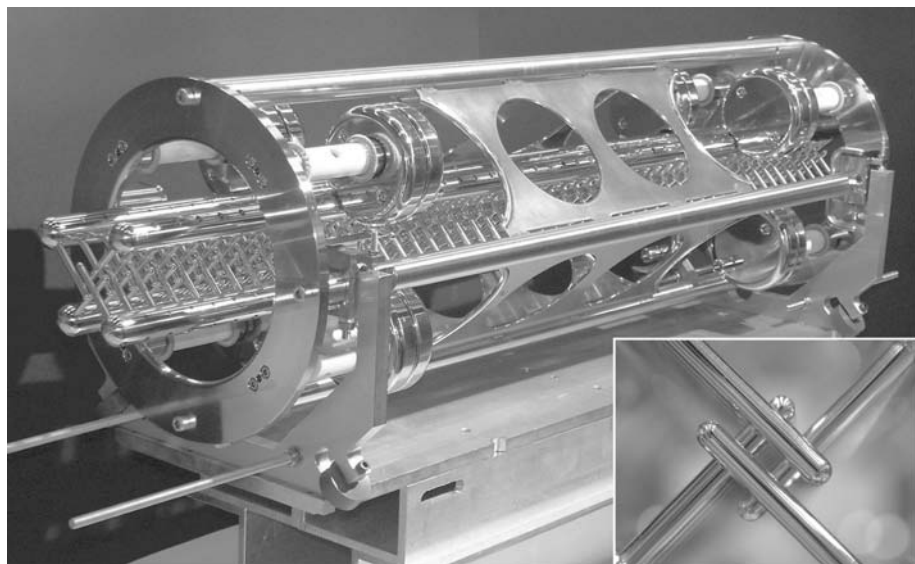
Figure 4 Picture of the Stark decelerator. The electric field stages are spaced 11 mm from each other. The length of the device is 1111 mm. The molecular beam passes through the 4×4 mm^2 opening area between the electrodes, which is shown enlarged in the inset. The molecules are decelerated by switching at the appropriate times a voltage difference of 40 kV between opposing electrodes.

high-voltage burst is typically 2–6 ms. In the remaining time before the next burst starts, the capacitor is charged by a 1.2 kW high-voltage power supply (Spellman SL1200) that is connected in series with a 26 kΩ loading resistor to the capacitor bank. The high-voltage push-pull switches switch between both voltage input ports upon application of a trigger pulse. The two voltage inputs are, in series with a 2.5 kΩ resistor, connected to ground and to the high-voltage capacitor bank, respectively. The decelerator represents a capacitance of approximately 120 pF. With a total resistance of 3 kΩ between the voltage supply and the decelerator, the voltage can be switched with a $1/e$ time of about 450 ns. During switching, a maximum current of approximately 13 A flows through the switch and the high-voltage circuitry. Each of the four-switch units is placed in a metal box that shields the generated radiation. The molecular beam machine runs at a repetition rate of 10 Hz. Every unit switches about 1000 times per second, and the total power that is dissipated in a unit is on the order of 150 W. Therefore, the resistors are cooled by small fans, and the switches are cooled by a 3 l min^{-1} oil (Galden ht 200) flow.

The last seven stages of the decelerator are electrically and mechanically decoupled from the first 101 stages and are operated with a separate set of high-voltage switches and power supplies. The advantage of this is that maximum flexibility is obtained, as these last stages are easily replaced or modified leaving the main decelerator intact. The limited number of electric field stages enables a compact design that is advantageous when the decelerator is to be used in combination with an electrostatic trap. In addition, the operation voltage of these last stages can be selected independently from the first 101 stages to reduce the risk of electrical breakdown between the decelerator and the electrostatic trap. A maximum voltage of ±15 kV is applied to these last stages, using a separate set of switches (Behlke Elektronik HTS 301-03-GSM) and power supplies (Spellman SL150). For these switch units, no oil or air cooling is required. The trigger pulses for the switches are generated by a programmable pulse generator, with a resolution of 100 ns. In total eight independent channels are available, where each channel can trigger a maximum of two switch units. The valve, lasers, and pulse generator are synchronized by a master clock (Stanford research DG535) running at a repetition rate of 10 Hz.

The OH radicals are state selectively detected inside the quadrupole trap, 21 mm downstream from the last electric field stage (1.307 m from the nozzle), using an off-resonant laser-induced fluorescence (LIF) detection scheme. The trap is described in detail in Section 4. All high voltages of the decelerator and hexapole are switched off 3 μs prior to detection. The 282 nm radiation of a pulsed dye laser (Spectra Physics INDI Nd:YAG laser/PDL3 dye laser combination) crosses the molecular beam at right angles. Optical access to the trap is provided by two 6 mm diameter holes in the ring electrode. The population of the low-field seeking $J = 3/2$ component of f parity is probed by inducing both the $Q_{21}(1)$ and the $Q_1(1)$ transitions of the $A^2\Sigma^+, v = 1 \leftarrow X^2\Pi_{3/2}, v = 0$ band. The population in both $M_J\Omega$ components of this level is probed simultaneously. Typically, 1.5 mJ of radiation in a 5 ns pulse with a 0.08 cm^{-1} bandwidth is used in a 5 mm

laser beam diameter, sufficient to saturate the transitions. The $A^2\Sigma^+$, $v = 1$ state has a radiative lifetime of 760 ns (79), and fluorescence occurs mainly via the $A^2\Sigma^+$, $v = 1 \rightarrow X^2\Pi_{3/2}$, $v = 1$ band around 313 nm. The LIF is imaged through a 6 mm diameter opening in the second end-cap onto a photomultiplier tube (PMT) (electron tubes B2/RFI, 9813 QB). Stray light from the laser is reduced by passing the laser beam through light baffles between the entrance and the exit windows. Stray light is further suppressed by optical filtering in front of the PMT.

The performance of the Stark decelerator is studied by recording the time-of-flight (TOF) profile of the OH radicals exciting the decelerator and by scanning the timing of the excitation laser relative to the dissociation laser. It is emphasized that in using photodissociation as the production method for the OH radicals, the beam is prepared at a well-defined position and time that is ideal for an accurate interpretation of the observed TOF profiles.

3.2. Guiding a Molecular Beam of OH Radicals

In the experiments described in this section, Kr is used as a carrier gas, producing a molecular beam with a mean velocity of 450 m s^{-1}. In the upper curve of Figure 5, the TOF profile shown is observed when the decelerator is operated at a phase angle of $\phi_0 = 0°$ for a velocity of the synchronous molecule of 450 m s^{-1}. Operation of the decelerator at $\phi_0 = 0°$ corresponds to a traveling potential well, moving with a constant velocity. The first pair of electrodes of the decelerator is switched to high voltage when the synchronous molecule for which the time sequence is calculated is exactly in between the first and second set of electrodes, thereby coupling in the beam at the center of the longitudinal acceptance region of the decelerator. The observed TOF profile clearly demonstrates that a significant fraction of the molecular beam, centered around the velocity of the potential well, is selected by the decelerator, transported through the machine, and arrives at the detector as a compact package, about 2.9 ms after production. The molecules in the beam that are not trapped by the traveling potential well experience the switched electric fields as well, resulting in rich phase-space dynamics that manifests itself by the features in the wings of the TOF profiles. From a calculation of the (time-dependent) electric-field distribution inside the decelerator, and by using the known Stark effect of OH, the trajectory of the OH molecules through the Stark decelerator can be simulated. The arrival time distribution that results from three-dimensional trajectory calculations of the experiment is shown directly underneath the experimental profile. It is seen that the simulations quantitatively reproduce the observations. From the calculations, the contributions of the individual $M_J\Omega$ components to the TOF profiles can be identified. The lower curves of Figure 5 show simulations of the individual contributions of the $M_J\Omega = -9/4$ and the $M_J\Omega = -3/4$ components to the TOF profile. In the simulations, both $M_J\Omega$ components of the OH ($J = 3/2$) state are taken into account, and it is assumed that directly after production both $M_J\Omega$ components are equally populated in the beam. The $M_J\Omega = -9/4$ contributes mainly to the main peak, reflecting
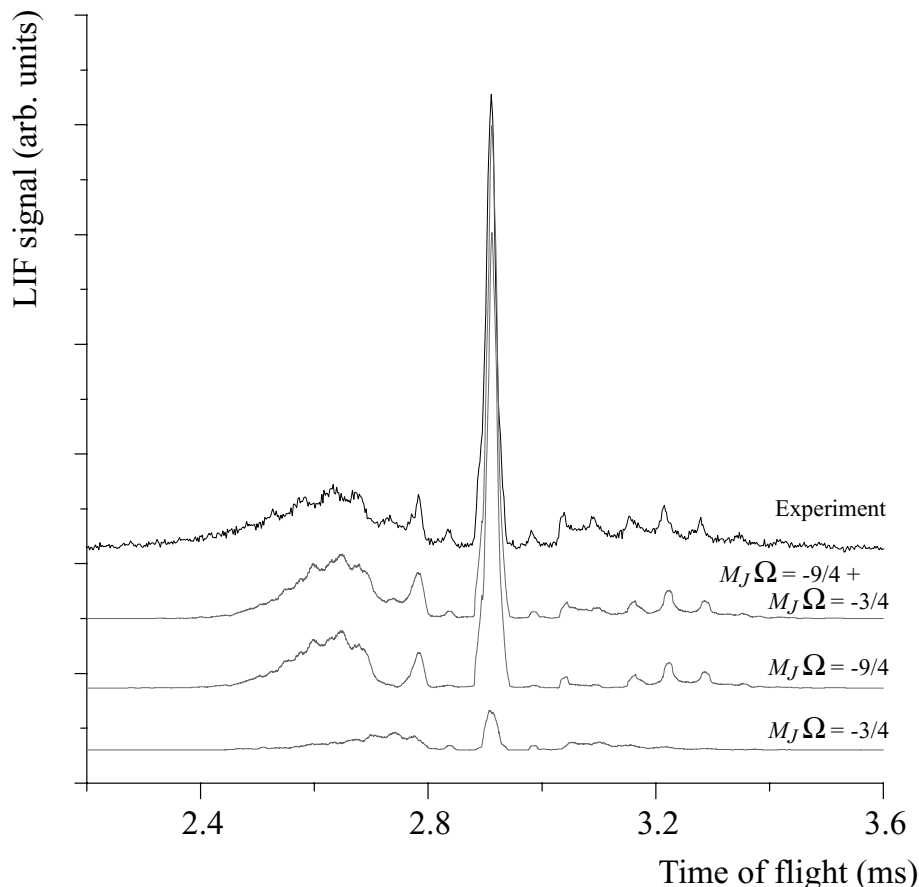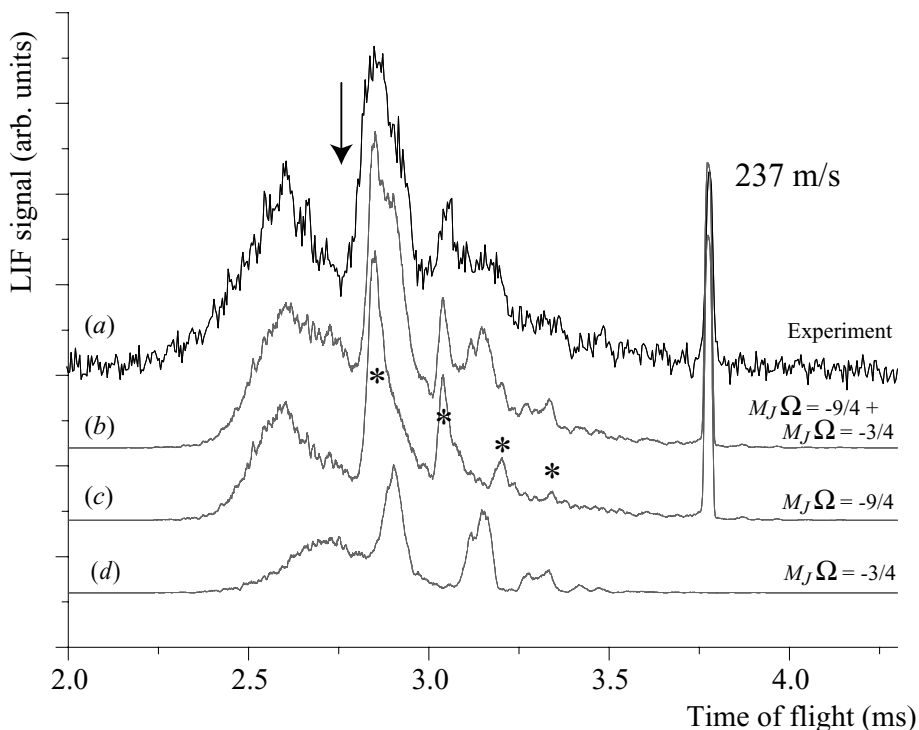
Figure 5 Observed TOF profile when the decelerator is operated at a phase angle $\phi_0 = 0°$ for a synchronous molecule with a velocity of 450 m s^{-1}. The TOF profile obtained from a three-dimensional trajectory simulation of the experiment is shown underneath the experimental profile. The individual contributions of both $M_J\Omega$ components of the OH ($^2\Pi_{3/2}, J = 3/2$) state to the overall profile are indicated.

the larger phase-space acceptance of the decelerator, and the more ideal focusing properties of the hexapole for this component. It is evident from Figure 5 that both $M_J\Omega$ components need to be taken into account to obtain a quantitative agreement between trajectory simulations and experimental data.

3.3. Deceleration of a Molecular Beam of OH Radicals

A part of the molecular beam can be decelerated when operating the decelerator at a phase angle $0° < \phi_0 < 90°$, decreasing the velocity of the potential well

Figure 6   LIF signal of OH ($J = 3/2$) radicals exiting the decelerator as a function of time after OH production (curve *a*). The decelerator is operated at a phase angle of $\phi_0 = 70°$ for a synchronous molecule with an initial velocity of 470 m s^{-1}. A significant fraction of the molecular beam is decelerated to 237 m s^{-1}. The TOF profile that results from a simulation of the experiment is shown in curve *b*, together with the individual contributions of both $M_J\Omega$ components to the profile (curves *c* and *d*).

gradually. The observed TOF profile is shown in Figure 6 (curve a) when the decelerator is operated with a time sequence that is calculated for a phase angle of $\phi_0 = 70°$ and for a synchronous molecule with an initial velocity of 470 m s^{-1}. With these settings, the decelerator extracts 1.1 cm^{-1} of kinetic energy from the synchronous molecule in every electric field stage. A selected fraction of the molecular beam is decelerated from 470 m s^{-1} (kinetic energy of 157 cm^{-1}) to a final velocity of 237 m s^{-1} (40 cm^{-1}) and is split off from the remaining part of the beam that is not decelerated. The decelerated bunch of molecules arrives in the LIF zone about 3.8 ms after production. The hole in the TOF profile of the fast beam due to the disappearance of OH radicals that are decelerated is indicated by an arrow. The improved spatial acceptance of this new generation Stark decelerator results in a peak intensity of the decelerated package similar to the peak intensity of the nondecelerated beam. The TOF profile obtained from a three-dimensional

trajectory simulation of the experiment is shown in curve b, together with the individual contributions of both $M_J\Omega$ components to the profile (curves c and d). The simulations quantitatively reproduce the observed TOF profile. As expected, the decelerated package purely consists of molecules in the $J = 3/2, M_J\Omega = -9/4$ state, but molecules in the $J = 3/2, M_J\Omega = -3/4$ state significantly contribute to the signal of the nondecelerated beam. The $M_J\Omega$ composition of the structured TOF profile of the nondecelerated beam is easily identified from the simulations. In addition, these calculations reveal the origin of the interesting structure of the nondecelerated beam that manifests itself for instance by the series of peaks indicated with a star in Figure 6 (curve c). A detailed discussion of the origin of these features is given in Section 3.4.

The molecular beam can be decelerated to lower final velocities by operating the decelerator at a higher phase angle, and/or by selecting a lower initial velocity of the synchronous molecule. The depth of the traveling potential well rapidly decreases for increasing values of ϕ_0. It is therefore advantageous to use a lower initial velocity instead. In Figure 7 a series of TOF profiles is shown that is obtained when the Stark decelerator is operated at a phase angle of $\phi_0 = 70°$ and an initial velocity of the synchronous molecule of 470 m s^{-1} (curve a), 450 m s^{-1} (curve b), 430 m s^{-1} (curve c), and 417 m s^{-1} (curve d). With these settings, the decelerated bunch of molecules exits the decelerator with a final velocity of 237 m s^{-1}, 194 m s^{-1}, 142 m s^{-1}, and 95 m s^{-1}, respectively. These measurements are complementary to the TOF profile shown in Figure 6 that is identical to Figure 7 (curve a). Again, the holes in the profiles of the nondecelerated beam that result from the removal of the bunches of OH radicals that are decelerated are indicated by the vertical arrows. As the width of the velocity distribution of the decelerated package only depends on the phase angle and not on the initial velocity of the synchronous molecule, the width of the arrival time distribution of the decelerated package becomes larger for lower values of the final velocity. Both the spreading out of the beam while flying from the exit of the decelerator to the LIF zone and the spatial extent of the detection laser beam are incorporated in the trajectory simulations of the experiments, shown underneath the observed profiles. In Figure 7 curves c and d, a rich oscillatory structure on the TOF profile of the fast beam is observed as shown enlarged in the figure. This structure results from a modulation of the phase-space distribution of the beam in the decelerator and is discussed in more detail elsewhere (49). In general, an excellent agreement between the trajectory simulations and the observed TOF profiles is obtained. The relative signal intensities of the different experimental TOF profiles, as well as the relative peak intensity of the decelerated beam and the fast beam within each profile, are quantitatively reproduced. This verifies that indeed the decelerator transports the selected package of molecules to lower velocities without loss. To date, no indications have been found for the occurrence of losses due to, for instance, Majorana transitions (80) or the re-projection of the $M_J\Omega = -9/4$ component onto the $M_J\Omega = -3/4$ component when the fields are switched.
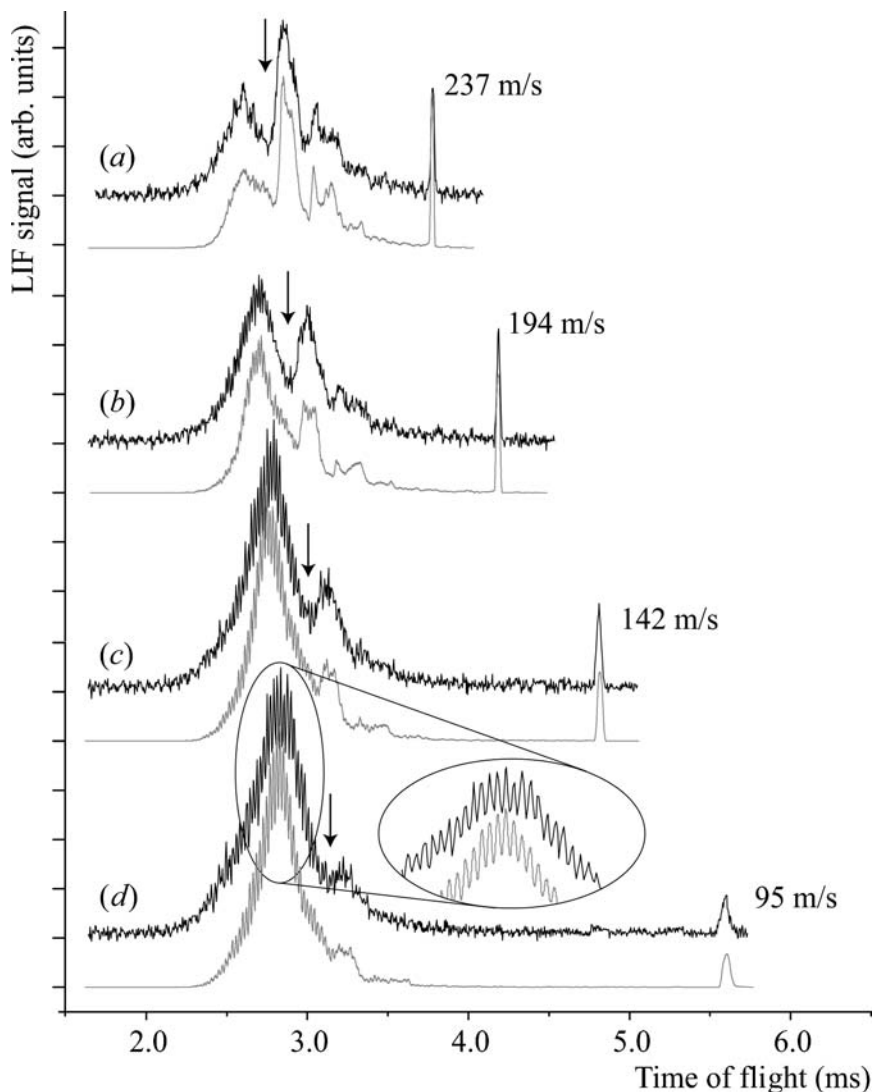
Figure 7   Observed and simulated TOF profiles of a molecular beam of OH radicals exiting the Stark decelerator when the decelerator is operated at a phase angle of $70°$ for a synchronous molecule with an initial velocity of 470 m s^{-1} (curve a), 450 m s^{-1} (curve b), 430 m s^{-1} (curve c), and 417 m s^{-1} (curve d). The molecules that are accepted by the decelerator are split off from the molecular beam and arrive at later times in the detection region.

Obviously, selecting a velocity that is lower than the mean velocity of the beam results in a lower phase-space density of the decelerated package than the peak phase-space density of the molecular beam. Using Xe as a carrier gas instead of Kr, the mean velocity of the beam can be reduced to approximately 365 m s^{-1}, enabling the operation of the decelerator at significantly lower phase angles. However, Xe enhances cluster formation in the expansion, resulting in a lower beam intensity. Together with the increased spreading out of the beam before the entrance of the Stark decelerator, this reduces the advantages of the lower initial velocity. From a sequence of experiments using Kr and Xe as carrier gases, it is found that Xe is superior if final velocities lower than approximately 150 m s^{-1} are required. In experiments described in Section 4, Xe is used as a carrier gas to decelerate a bunch of OH radicals to a final velocity of approximately 20 m s^{-1} before loading them into an electrostatic quadrupole trap.

3.4. Evolution of the Beam Through the Stark Decelerator

In addition to demonstrating the operation principle of a decelerator, the TOF profiles of Figures 5 and 7 indicate rich phase-space dynamics of the untrapped molecules as well. A detailed understanding of the dynamics of the beam in the decelerator, both of the part that undergoes phase-stable oscillations and of the molecules that are not trapped, can be obtained from the trajectory simulations. These simulations accurately reproduce the observed TOF profiles; the calculated phase-space distributions should therefore be realistic as well. The details of the evolution of the phase-space distribution of the beam throughout the deceleration process will depend on the exact settings of the decelerator, but a good understanding of the general features can be obtained by studying two limiting cases.

In this section, we discuss the progression of the beam inside the decelerator, if the decelerator is operated with a time sequence that corresponds to the guiding experiment presented in Figure 5 (the decelerator is operated at phase angle $\phi_0 = 0°$) and to the deceleration experiment shown in Figure 6 ($\phi_0 = 70°$). To test the validity of the (one-dimensional) model presented in Section 2.2, one-dimensional trajectory simulations are carried out for a beam of OH radicals that are exclusively in the $J = 3/2$, $M_J\Omega = -9/4$ state. The influence of transverse effects on the longitudinal phase-space distributions has recently been discussed in detail elsewhere (51).
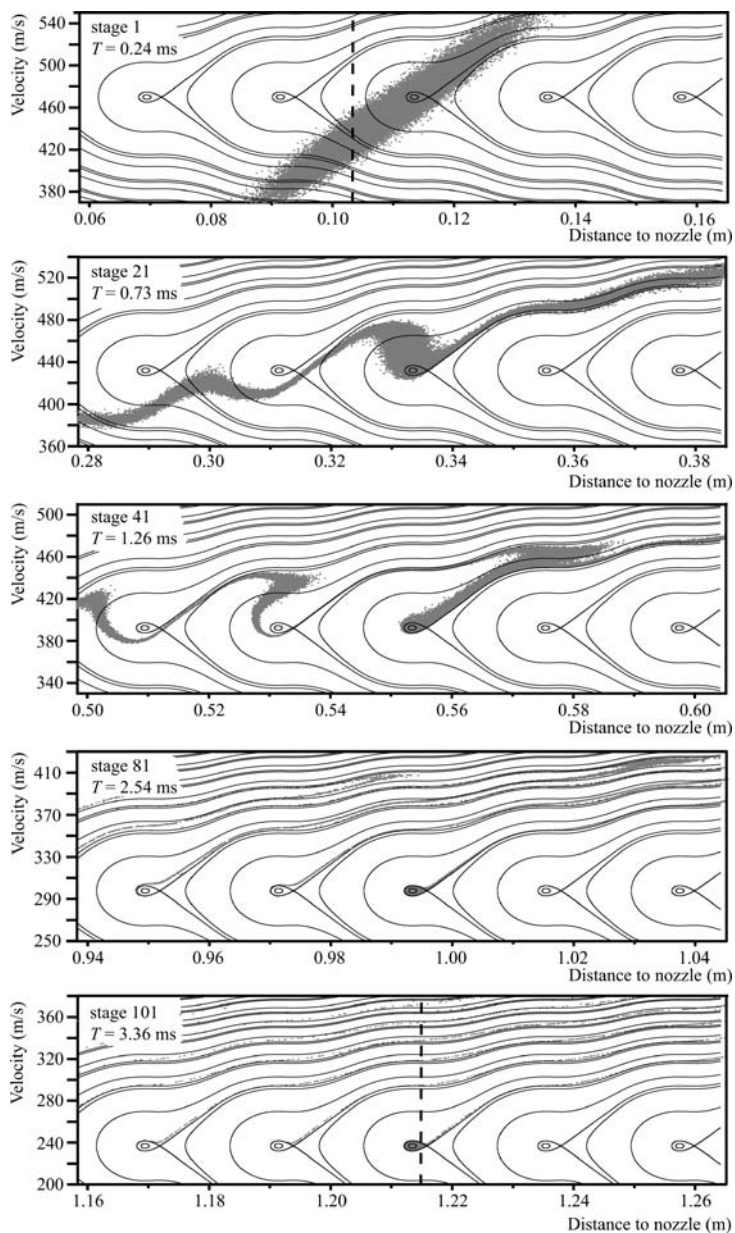
Figure 8 shows the evolution of the longitudinal phase-space distribution of the beam of OH ($M_J\Omega = -9/4$) radicals that results from a one-dimensional trajectory calculation of the measurement presented in Figure 5. The decelerator is operated at a phase angle $\phi_0 = 0°$ for a synchronous molecule with an initial velocity of 450 m s^{-1}. The phase-space distribution is shown at the switch time when the synchronous molecule is in stage 1 ($T = 0.23$ ms after production of the beam), stage 21 ($T = 0.72$ ms), stage 41 ($T = 1.21$ ms), stage 81 ($T = 2.19$ ms), and stage 101 ($T = 2.68$ ms) of the Stark decelerator. In this notation, stage i represents the region in the decelerator between electrode pairs i and $i + 1$.
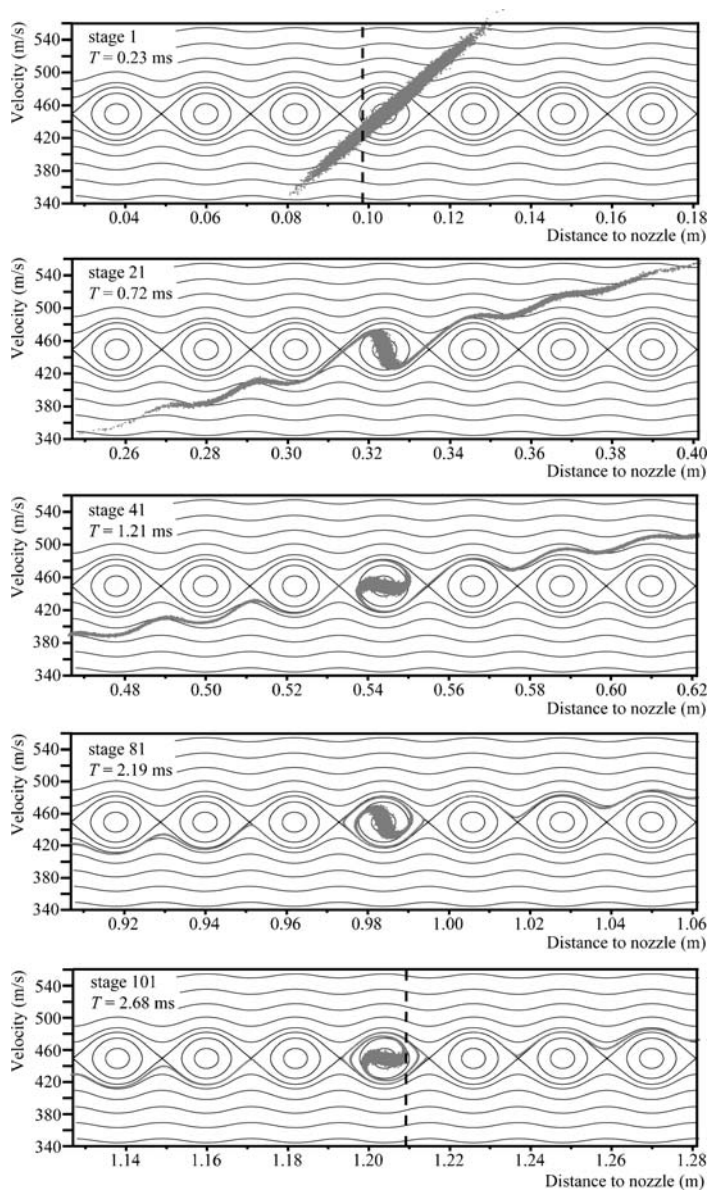
Figure 8 Evolution of the longitudinal phase-space distribution of the beam of OH ($M_J\Omega = -9/4$) radicals that results from a one-dimensional trajectory calculation of the measurement shown in Figure 5. The decelerator is operated at a phase angle $\phi_0 = 0°$. The distribution is shown at the switch time when the synchronous molecule is in stage 1, 21, 41, 81, and 101 of the Stark decelerator. The entrance and exit of the decelerator are indicated by the dashed lines.

The entrance (center of electrode pair 1) and exit (center of electrode pair 102) are indicated by vertical dashed lines. The phase-space diagrams that result from the model presented in Section 2.2 are given as an overlay. In the simulations, we assume that just after production ($T = 0.00$ ms), the beam has a Gaussian velocity profile with a mean velocity of 450 m s^{-1} and a velocity spread of 15%. The longitudinal position spread is determined by the width of the dissociation laser focus, and a Gaussian profile with a width of 4 mm is assumed. This results in a vertical phase-space distribution at the position of the nozzle orifice (phase-space distribution not shown). The upper graph in Figure 8 shows the phase-space distribution of the beam at $T = 0.23$ ms. At this time, the most intense part of the molecular beam is at the center of the first electric field stage, and the first high-voltage pulse is applied to the Stark decelerator. The tilted phase-space distribution results from the free flight of the beam from the production region to the Stark decelerator. It is seen that the longitudinal acceptance of the decelerator encompasses a significant fraction of the emittance of the molecular beam. At $T = 0.72$ ms, the synchronous molecule has progressed to stage 21 in the decelerator. Molecules within the separatrix (bucket) have rotated around the synchronous molecule. Molecules outside this bound region follow the lines of constant energy in the phase-space diagram, resulting in a pronounced modulation of the phase-space distribution of the beam. This modulation represents the influence of the switched electric fields on the molecules that are not trapped by the traveling potential well. In fact, the regions where the modulated distribution is horizontal give rise to the small peaks in the wings of the TOF profiles of Figure 5. The trajectory of the molecules outside the separatrix is unstable, and the corresponding fraction of the molecular beam will continue to spread out as it progresses through the decelerator. This becomes increasingly apparent in the phase-space distributions at $T = 1.21$ ms (stage 41), $T = 2.19$ ms (stage 81), and $T = 2.68$ ms (stage 101). In Figure 8, only a selected fraction of the phase-space distribution of the beam is shown for reasons of clarity. The bound molecules continue to rotate around the synchronous molecule and are kept together throughout the decelerator. The unbound molecules spread out in position and approach the separatrices of the buckets in front of and behind the bucket that contains the stable molecules. Obviously, for an infinite decelerator, the density of the unbound molecules will approach zero, resulting in a TOF profile that consists of a sharp narrow peak on a zero signal baseline. For the decelerator used in the present experiments, the 101 electric field stages used are sufficient to diminish the density of the beam close to the first neighboring separatrices to an undetectable value, as is seen in Figure 5 by the region of zero signal in the TOF profiles on either side of the main peak.

In analogy to Figure 8, the longitudinal phase-space dynamics of a beam of OH ($J = 3/2$, $M\Omega = -9/4$) radicals is depicted in Figure 9, for settings of the decelerator that correspond to the deceleration experiment shown in Figure 6. The Stark decelerator is operated at a phase angle of $\phi_0 = 70°$ for a synchronous molecule with an initial velocity of 470 m s^{-1}, and the corresponding phase-space

Figure 9 Evolution of the longitudinal phase-space distribution of the beam of OH ($M_J\Omega = -9/4$) radicals that results from a one-dimensional trajectory calculation of the deceleration experiment shown in Figure 6. The decelerator is operated at a phase angle $\phi_0 = 70°$ for a synchronous molecule with an initial velocity of 470 m s^{-1}.

diagrams of the decelerator are given as an overlay. The upper graph shows the distribution at $T = 0.24$ ms, when the synchronous molecule is at the center of the phase-stable region in the first electric field stage of the decelerator. The center position of the first pair of electrodes is again indicated by the vertical dashed line. The nozzle-to-skimmer distance used in this experiment is slightly larger than in the guiding experiment. In the discussion of the progression of the beam through the decelerator, three different regions in the phase-space distribution of the beam in stage 1 are considered separately, namely (*a*) molecules that are within the bucket bound by the separatrix; (*b*) the part of the beam that is in position, and therefore also in velocity, ahead of the bucket; and (*c*) the part of the beam that lags behind. The molecules within the bucket (part *a*) are phase stable and oscillate around the velocity and phase of the synchronous molecule. The size of the separatrix is sufficiently small so that the bucket is completely filled with molecules, and the spiral-like structure occurring in Figure 8 is absent. The separatrix accurately describes the shape of the phase-stable region, and the selected bunch of molecules leaves the decelerator with a velocity of 237 m s^{-1}, 3.36 ms after production of the beam.

Analogous to operating the decelerator at $\phi_0 = 0°$, the part of the beam that was initially too fast (part *b*) is modulated by the presence of empty buckets along the length of the entire decelerator. When the beam overtakes the position of a bucket, the interaction with the fields results in a horizontal phase-space distribution, ultimately leading to a peak in the TOF distribution. However, the pronounced oscillatory structure in the observed TOF profiles of the nondecelerated beam, shown enlarged in Figure 7, cannot be understood from this alone and a full understanding of these oscillations is only obtained when higher-order effects are included in the model (49).

Molecules just outside the bucket and that are initially too slow (part *c*) are not captured by the decelerating potential well and follow the curves of equal energy in the phase-space diagrams. These molecules accelerate with respect to the synchronous molecule, as can be seen from the phase-space distribution of the beam at $T = 0.73$ ms (stage 21). Molecules that were initially even slower start interacting with the empty buckets that lag behind. The beam cannot penetrate into the stable area and evolves around the separatrix of the corresponding bucket. This leads to turning points in the phase-space distribution of the beam, which are most apparent in the diagram in Figure 9 that corresponds to $T = 1.26$ ms (stage 41). These turning points result in the series of peaks in the TOF profile of the nondecelerated beam, indicated by stars in Figure 6. The tail in the distribution that connects the filled bucket containing the trapped package and the corresponding turning point becomes increasingly longer and less dense as the velocity of the synchronous molecule decreases. At $T = 2.54$ ms, the decelerated package has a velocity close to 290 m s^{-1} and is almost completely decoupled from the part of the beam that is not decelerated. At this time, the fastest molecules in the beam have already reached the detection zone.

4. ELECTROSTATIC TRAPPING OF OH RADICALS

To exploit the possibilities that this new Stark decelerator offers to study molecules at (ultra-)low temperatures and for collision and reactive scattering experiments at these temperatures, the slow beam needs to be decelerated further and confined in a trap. For this, the decelerator is extended with an electrostatic quadrupole trap (11, 14) (Figure 3). The trap consists of a ring electrode, centered 21 mm downstream from the last electrodes of the decelerator, with an inner radius R of 10 mm and two hyperbolic end-caps with a half-spacing of $R/\sqrt{2}$. This trap is scaled up by a factor 2 compared with the trap used to trap ND_3 molecules (11, 14). The molecular beam enters the trap through a 4-mm-diameter hole in the first end-cap. This hole is the only vacuum connection between the deceleration chamber and the trap chamber, and the pressure in the trap chamber can be kept at approximately 3×10^{-9} torr under operating conditions. The OH radicals are detected inside the trap using the detection scheme described above.

To be able to load the OH radicals into the electrostatic trap, the beam needs to be decelerated to approximately 20 m s^{-1}. This can best be achieved when Xe is used as a carrier gas, producing a molecular beam with a mean velocity of 360 m s^{-1}. Figure 10 shows the observed TOF profile when the first 101 stages of the decelerator are operated at $\phi_0 = 53°$, extracting approximately 0.9 cm^{-1}
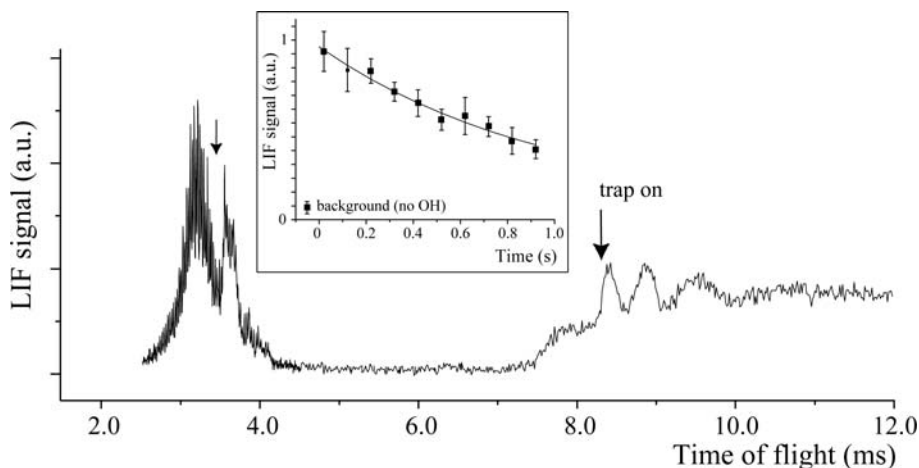
Figure 10   LIF signal of OH ($J = 3/2$) radicals at the center of the quadrupole trap as a function of time after OH production for a deceleration and trapping sequence. The synchronous molecule is decelerated from the initial velocity of 371 m s^{-1} to a standstill. The hole in the TOF profile of the fast beam due to the removal of OH radicals that are decelerated is indicated by an arrow. The time at which the trap is switched on is indicated by a vertical arrow as well. In the inset, the LIF signal intensity of the electrostatically trapped OH radicals is shown on a longer timescale.

Loading geometry   Trapping geometry
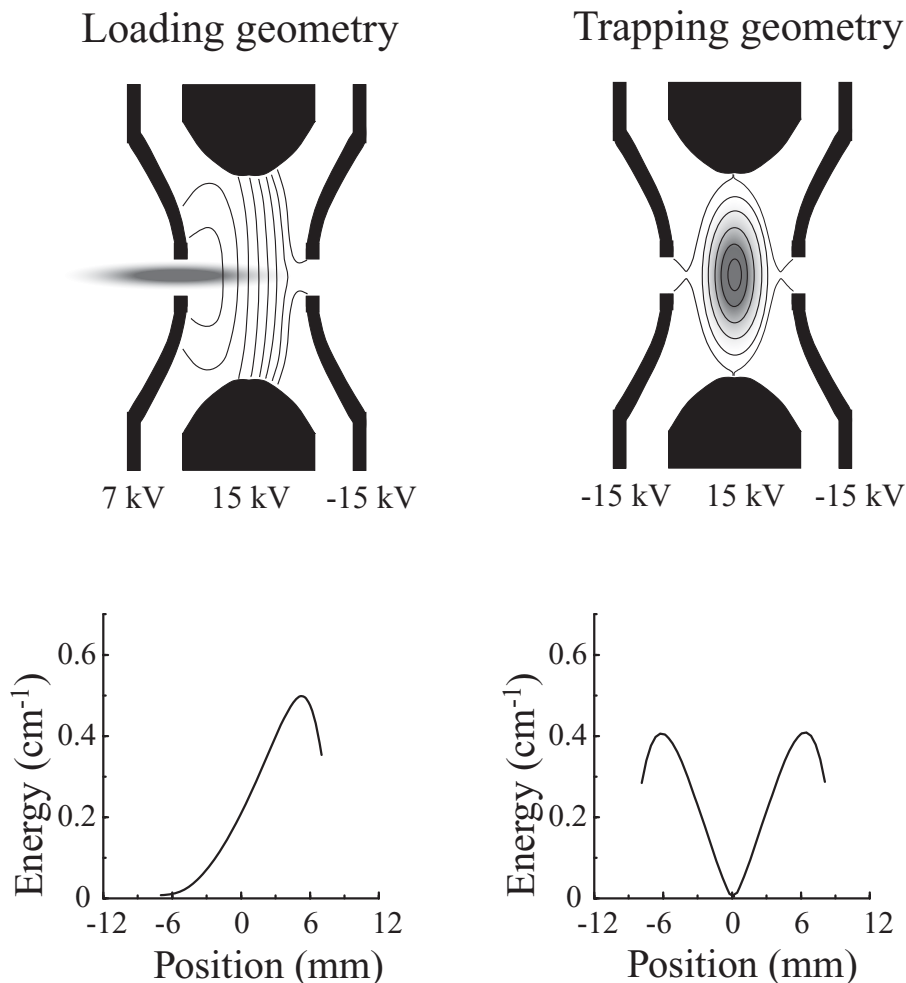
Figure 11 A schematic representation of the loading procedure of the electrostatic trap. In the loading geometry, the potentials on the trap electrodes are chosen such that a potential hill is created in the trap that is higher than the remaining kinetic energy of the incoming molecules. At the time the molecules come to a standstill at the center of the trap, the trap is switched into the trapping geometry. In this geometry, a (nearly) symmetric 500 mK deep potential well is created, in which the molecules are confined.

of kinetic energy per deceleration stage. OH radicals with an initial velocity of 371 m s^{-1} ($E_{\text{kin}} = 97.8$ cm^{-1}) are decelerated to a velocity of 84 m s^{-1} in stage 101. The last seven stages can only be used with a maximum voltage difference of 30 kV between the electrodes in a deceleration stage. These stages are operated at the lower phase angle of $\phi_0 = 48°$ to compensate for the reduced acceptance of

the decelerator in these last stages. Here, the decelerator extracts approximately 0.6 cm^{-1} of kinetic energy per deceleration stage, and the OH radicals exit the decelerator with a velocity of approximately 21 m s^{-1} ($E_{kin} = 0.3$ cm^{-1}).

The slow beam of OH radicals is loaded into the electrostatic trap with voltages of 7 kV, 15 kV, and −15 kV on the first end-cap, the ring electrode, and the second end-cap, respectively. This so-called loading geometry of the trap is schematically represented on the left side of Figure 11. In the loading geometry, a potential hill in the trap is created that is higher than the remaining kinetic energy of the molecules. The OH radicals therefore come to a standstill near the center of the trap, approximately 8.3 ms after their production. At that time, indicated by an arrow in Figure 10, the trap is switched into the so-called trapping geometry, as schematically represented on the right side of Figure 11; the first end-cap is switched from 7 kV to −15 kV to create a (nearly) symmetric 500 mK deep potential well. After some initial oscillations, a steady LIF signal is observed from the OH radicals in the trap. The LIF intensity of the trapped OH radicals is approximately 40% of the peak LIF intensity of the nondecelerated beam of OH that passes through the trap. The hole in the TOF profile of the fast beam, due to the removal of OH radicals that are decelerated, is again indicated by an arrow.

Quantifying LIF signals is notoriously difficult. The observed LIF signal of the trapped OH radicals corresponds to a total number of approximately 10^5 OH ($J = 3/2$, $M_J\Omega = -9/4$) radicals, in the approximately 0.03 cm^3 detection volume in the trap. The inset of Figure 10 shows the LIF signal intensity on a longer timescale. The latter experiments are performed while running the experiment at a repetition rate of 1 Hz, limiting the maximum trapping time that can be measured to 1.0 s. From these experiments, a $1/e$ trap lifetime on the order of 1.0 s, limited by collisions with background gas, is deduced. The absolute number of OH radicals that can be trapped, as well as the phase-space distribution of the trapped molecules, critically depends on the details of the trap-loading sequence (81). Depending on the loading characteristics, the density of the trapped cloud is approximately 10^7–10^8 cm^{-3}, and the temperature can be as low as 50 mK.

5. CONCLUSIONS

In this review, we describe a Stark decelerator designed to capture and slow down a large fraction of a molecular beam. Deceleration experiments are performed using a beam of OH radicals, a chemically highly relevant species. We study in detail both the deceleration process and the phase-space dynamics of the molecules that are not phase stable. The Stark decelerator is extended with an electrostatic trap in which the selected part of the molecular beam can be brought to a standstill and stored up to seconds. The produced cold packages of OH radicals are ideally suited to study cold (reactive) collisions between the trapped polar molecules, which is a very new and exciting field of physics. At present, however, the density of

10^7–10^8 OH radicals cm^{-3} that we have reached is not sufficient to observe these collisions in the trap. By improving the deceleration and trap-loading process, it is estimated that approximately an order of magnitude can be gained in density. If a more intense molecular beam can be produced, the density could be enhanced even further. Using state-of-the-art molecular beam techniques, densities exceeding 10^{10} molecules cm^{-3} should therefore be realistic. Once these densities are obtained, methods such as evaporative cooling or sympathetic cooling could be applied to cool down the trapped sample further and hence increase the phase-space density in the trap. These methods have not yet been demonstrated to work for molecules and rely on the (presently unknown) elastic and inelastic collision cross sections. Also direct laser cooling prior to the loading of the trap could be used to cool the sample. An alternative approach to increase the phase-space density in the trap is to accumulate several packages of molecules in the trap, which is possible in specific systems (82, 83).

ACKNOWLEDGMENTS

**The *Annual Review of Physical Chemistry* is online at
http://physchem.annualreviews.org**

LITERATURE CITED

1. Scoles G, ed. 1988/1992. *Atomic and Molecular Beam Methods*, Vols. 1, 2. New York: Oxford Univ. Press

2. Stapelfeldt H, Seideman T. 2003. Colloquium: aligning molecules with strong laser pulses. *Rev. Mod. Phys.* 75:543–57

3. Yang X, Liu K, eds. 2004. *Modern Trends in Chemical Reaction Dynamics*, Vol. 1. Singapore: World Sci.

4. Sato H. 2001. Photodissociation of simple molecules in the gas phase. *Chem. Rev.* 101:2687–725

5. Rakitzis TP, van den Brom AJ, Janssen MHM. 2004. Directional dynamics in the photodissociation of oriented molecules. *Science* 303:1852–54

6. Liu K. 2001. Crossed-beam studies of neutral reactions: State-specific differential cross sections. *Annu. Rev. Phys. Chem.* 52:139–64

7. Lin JJ, Zhou J, Shiu W, Liu K. 2003. State-specific correlation of coincident product pairs in the F + CD$_4$ reaction. *Science* 300:966–69

8. Bethlem HL, Berden G, Meijer G. 1999. Decelerating neutral dipolar molecules. *Phys. Rev. Lett.* 83:1558–61

9. Bethlem HL, van Roij AJA, Jongma RT, Meijer G. 2002. Alternate gradient focusing and deceleration of a molecular beam. *Phys. Rev. Lett.* 88(13):133003

10. Crompvoets FMH, Jongma RT, Bethlem

HL, van Roij AJA, Meijer G. 2002. Longitudinal focusing and cooling of a molecular beam. *Phys. Rev. Lett.* 89(9):093004

11. Bethlem HL, Berden G, Crompvoets FMH, Jongma RT, van Roij AJA, Meijer G. 2000. Electrostatic trapping of ammonia molecules. *Nature* 406:491–94

12. van Veldhoven J, Bethlem HL, Meijer G. 2005. AC electric trap for ground-state molecules. *Phys. Rev. Lett.* 94:083001

13. Crompvoets FMH, Bethlem HL, Jongma RT, Meijer G. 2001. A prototype storage ring for neutral molecules. *Nature* 411:174–76

14. Bethlem HL, Crompvoets FMH, Jongma RT, van de Meerakker SYT, Meijer G. 2002. Deceleration and trapping of ammonia using time-varying electric fields. *Phys. Rev. A* 65(5):053416

15. Bethlem HL, Meijer G. 2003. Production and application of translationally cold molecules. *Int. Rev. Phys. Chem.* 22(1):73–128

16. 2004. *Special Issue: Ultracold Polar Molecules: Formation and Collision. Eur. Phys. J. D* 31(2)

17. Hunter LR. 1991. Tests of time-reversal invariance in atoms, molecules, and the neutron. *Science* 252:73–79

18. Hudson JJ, Sauer BE, Tarbutt MR, Hinds EA. 2002. Measurement of the electron electric dipole moment using YbF molecules. *Phys. Rev. Lett.* 89:023003

19. Kawall D, Bay F, Bickman S, Jiang Y, DeMille D. 2004. Precision Zeeman–Stark spectroscopy of the metastable $a(1)^3\Sigma^+$ state of PbO. *Phys. Rev. Lett.* 92:133007

20. Rein DW. 1974. Some remarks on parity violating effects of intramolecular interactions. *J. Mol. Evol.* 4:15–22

21. Letokhov VS. 1975. On difference of energy levels of left and right molecules due to weak interactions. *Phys. Lett. A* 53:275–76

22. Uzan J-P. 2003. The fundamental constants and their variation: observational and theoretical status. *Rev. Mod. Phys.* 75:403–55

23. van de Meerakker SYT, Vanhaecke N, van der Loo MPJ, Groenenboom GC, Meijer G. 2005. Direct measurement of the radiative lifetime of vibrationally excited OH radicals. *Phys. Rev. Lett.* 95:013003

24. Wennberg PO, Cohen RC, Stimpfle RM, Koplow JP, Anderson JG, et al. 1994. Removal of stratospheric O_3 by radicals: In situ measurements of OH, HO_2, NO, NO_2, ClO and BrO. *Science* 266:398–404

25. Wennberg PO, Hanisco TF, Jaeglé L, Jacob DJ, Hintsa EJ, et al. 1998. Hydrogen radicals, nitrogen radicals, and the production of O_3 in the upper troposphere. *Science* 279:49–53

26. Summers ME, Conway RR, Siskind DE, Stevens MH, Offermann D, et al. 1997. Implications of satellite OH observations for middle atmospheric H_2O and ozone. *Science* 277:1967–70

27. Wilson WJ, Barrett AH. 1968. Discovery of hydroxyl radio emission from infrared stars. *Science* 161:778–79

28. Chu S. 1998. The manipulation of neutral particles. *Rev. Mod. Phys.* 70:685–706

29. Cohen-Tannoudji CN. 1998. Manipulating atoms with photons. *Rev. Mod. Phys.* 70:707–19

30. Phillips WD. 1998. Laser cooling and trapping of neutral atoms. *Rev. Mod. Phys.* 70:721–41

31. 2002. Special Issue. *Nature Insight: Ultracold Matter. Nature* 416:205–46

32. Anderson MH, Ensher JR, Matthews MR, Wieman CE, Cornell EA. 1995. Observation of Bose–Einstein condensation in a dilute atomic vapor. *Science* 269:198–201

33. Baranov M, Dobrek L, Goral K, Santos L, Lewenstein M. 2002. Ultracold dipolar gases—a challenge for experiments and theory. *Phys. Scr. T* 102:74–81

34. Santos L, Shlyapnikov GV, Soller P, Lewenstein M. 2000. Bose–Einstein condensation in trapped dipolar gases. *Phys. Rev. Lett.* 85:1791–94

35. Goral K, Santos L, Lewenstein M. 2002. Quantum phases of dipolar bosons in optical lattices. *Phys. Rev. Lett.* 88:170406

36. DeMille D. 2002. Quantum computation with trapped polar molecules. *Phys. Rev. Lett.* 88:067901

37. Herschbach D. 1999. Chemical physics: Molecular clouds, clusters and corrals. *Rev. Mod. Phys.* 71:S411–18

38. Balakrishnan N, Dalgarno A. 2001. Chemistry at ultracold temperatures. *Chem. Phys. Lett.* 341(5–6):652–56

39. Balakrishnan N, Dalgarno A, Forrey RC. 2000. Vibrational relaxation of CO by collisions with ^{4}He at ultracold temperatures. *J. Chem. Phys.* 113:621–27

40. King JG. 1959. Experiments with slow molecules. *Proc. 13th Annu. Symp. Frequency Control, Ashbury Park.* U.S. Army Signal Res. Dev. Lab., Fort Monmouth, p. 603

41. King JG, Zacharias JR. 1958. *Q. Progress Rep.*, Res. Lab. Electron., MIT, No. 48, Jan. 15

42. Oraevskii AN. 1964. *Molecular Generators*. Moscow: Nauka

43. Kazachok VS. 1965. The electrodynamic method of slowing down molecules. *Sov. Phys. Tech. Phys.* 10:882

44. Golub R. 1967. *On decelerating molecules*. PhD thesis. MIT

45. Auerbach D, Bromberg EEA, Wharton L. 1966. Alternate-gradient focusing of molecular beams. *J. Chem. Phys.* 45:2160–66

46. Wolfgang R. 1968. Chemical accelerators. *Sci. Am.* 219(4):44

47. Bromberg EEA. 1972. *Acceleration and alternate-gradient focusing of neutral polar diatomic molecules*. PhD thesis. Univ. Chicago

48. Bethlem HL, Berden G, van Roij AJA, Crompvoets FMH, Meijer G. 2000. Trapping neutral molecules in a traveling potential well. *Phys. Rev. Lett.* 84:5744–47

49. van de Meerakker SYT, Vanhaecke N, Bethlem HL, Meijer G. 2005. Higher-order resonances in a Stark decelerator. *Phys. Rev. A* 71:053409

50. Friedrich B. 2004. A quasi-analytical model for a linear Stark accelerator/ decelerator for polar molecules. *Eur. Phys. J. D* 31:313–36

51. van de Meerakker SYT, Vanhaecke N, Bethlem HL, Meijer G. 2006. Transverse stability in a Stark decelerator. *Phys. Rev. A*. In press

52. Crompvoets FMH, Bethlem HL, Küpper J, van Roij AJA, Meijer G. 2004. Dynamics of neutral molecules stored in a ring. *Phys. Rev. A* 69(6):063406

53. van Veldhoven J, Küpper J, Bethlem HL, Sartakov B, van Roij AJA, Meijer G. 2004. Decelerated molecular beams for high-resolution spectroscopy: The hyperfine structure of ^{15}ND$_3$. *Eur. Phys. J. D* 31(2):337–49

54. Bohn JL. 2001. Inelastic collisions of ultracold polar molecules. *Phys. Rev. A* 63: 052714

55. Schulz SA, Bethlem HL, van Veldhoven J, Küpper J, Conrad H, Meijer G. 2004. Microstructured switchable mirror for polar molecules. *Phys. Rev. Lett.* 93(2):020406

56. Tarbutt MR, Bethlem HL, Hudson JJ, Ryabov VL, Ryzhov VA, et al. 2004. Slowing heavy, ground-state molecules using an alternating gradient decelerator. *Phys. Rev. Lett.* 92(17):173002

57. Bochinski JR, Hudson ER, Lewandowski HJ, Meijer G, Ye J. 2003. Phase space manipulation of cold free radical OH molecules. *Phys. Rev. Lett.* 91:243001

58. Bochinski JR, Hudson ER, Lewandowski HJ, Ye J. 2004. Cold free-radical molecules in the laboratory frame. *Phys. Rev. A* 70: 043410

59. Deleted in proof

60. Yamakita Y, Procter SR, Goodgame AL, Softley TP. 2004. Deflection and deceleration of hydrogen Rydberg molecules in inhomogeneous electric fields. *J. Chem. Phys.* 121:1419–31

61. Vliegen E, Wörner HJ, Softley TP, Merkt F. 2004. Nonhydrogenic effects in the deceleration of Rydberg atoms in inhomogeneous electric fields. *Phys. Rev. Lett.* 92:033005

62. Vanhaecke N, Comparat D, Pillet P. 2005.

Rydberg decelerator using a travelling electric field gradient. *J. Phys. B* 38:409–19

63. Rangwala SA, Junglen T, Rieger T, Pinkse PWH, Rempe G. 2003. Continuous source of translationally cold dipolar molecules. *Phys. Rev. A* 67:043406

64. Deleted in proof

65. Junglen T, Rieger T, Pinkse PWH, Rempe G. 2004. Two-dimensional trapping of dipolar molecules in time-varying electric fields. *Phys. Rev. Lett.* 92:223001

66. Barker PF, Shneider MN. 2002. Slowing molecules by optical microlinear deceleration. *Phys. Rev. A* 66:065402

67. Dong GJ, Lu WP, Barker PF. 2004. Decelerating and bunching molecules with pulsed traveling optical lattices. *Phys. Rev. A* 69:013409

68. Fulton R, Bishop AI, Barker PF. 2004. Optical Stark decelerator for molecules. *Phys. Rev. Lett.* 93:243004

69. Wardle M, Yusef-Zadeh F. 2002. Supernova remnant OH masers: Signposts of cosmic collision. *Science* 296:2350–54

70. Miller JA, Kee RJ. 1990. Chemical kinetics and combustion modeling. *Annu. Rev. Phys. Chem.* 41:345–87

71. Whitehead JC. 1996. Molecular beam studies of free-radical processes: Photodissociation, inelastic and reactive collisions. *Rep. Prog. Phys.* 59:993–1040

72. Avdeenkov AV, Bohn JL. 2002. Collisional dynamics of ultracold OH molecules in an electrostatic field. *Phys. Rev. A* 66:052718

73. Avdeenkov AV, Bohn JL. 2003. Linking ultracold polar molecules. *Phys. Rev. Lett.* 90(4):043006

74. Avdeenkov AV, Bortolotti DCA, Bohn JL. 2004. Field-linked states of ultracold polar molecules. *Phys. Rev. A* 69:012710

75. Ticknor C, Bohn JL. 2005. Influence of magnetic fields on cold collisions of polar molecules. *Phys. Rev. A* 71:022709

76. Avdeenkov AV, Bohn JL. 2005. Ultracold collisions of fermionic OD radicals. *Phys. Rev. A* 71:022706

77. Anderson RW. 1997. Tracks of symmetric top molecules in hexapole electric fields. *J. Phys. Chem. A* 101:7664–73

78. Jongma RT, Rasing Th, Meijer G. 1995. Two-dimensional imaging of metastable CO molecules. *J. Chem. Phys.* 102(5):1925–33

79. Yarkony DR. 1992. A theoretical treatment of the predissociation of the individual rovibronic levels of OH/OD (A $^2\Sigma^+$). *J. Chem. Phys.* 97:1838–49

80. Harland PW, Hu WP, Vallance C, Brooks PR. 1999. Spatial deorientation of upper-stark-state-selected supersonic beams of CH_3F -Cl -Br and -I. *Phys. Rev. A* 60:3138–43

81. van de Meerakker SYT, Smeets PHM, Vanhaecke N, Meijer G. 2005. Deceleration and electrostatic trapping of OH radicals. *Phys. Rev. Lett.* 94:23004

82. van de Meerakker SYT, Jongma RT, Bethlem HL, Meijer G. 2001. Accumulating NH radicals in a magnetic trap. *Phys. Rev. A* 64:041401

83. van de Meerakker SYT, Sartakov BG, Mosk AP, Jongma RT, Meijer G. 2003. Optical pumping of metastable NH radicals into the paramagnetic ground state. *Phys. Rev. A* 68:032508

Contents

ERRATA
An online log of corrections to *Annual Review of Physical Chemistry*
chapters may be found at http://physchem.annualreviews.org/errata.shtml